



# Exploiting Supramolecular Interactions from Polymeric Colloids for Strong Anisotropic Adhesion between Solid Surfaces


Blaise L. Tardy,\* Joseph J. Richardson, Luiz G. Greca, Junling Guo, Hirotaka Ejima,\* and Orlando J. Rojas\*

Adhesion occurs by covalent bonding, as in reactive structural adhesives, or through noncovalent interactions, which are nearly ubiquitous in nature. A classic example of the latter is gecko feet, where hierarchical features enhance friction across the contact area. Biomimicry of such structured adhesion is regularly achieved by top-down lithography, which allows for direction-dependent detachment. However, bottom-up approaches remain elusive given the scarcity of building blocks that yield strong, cohesive, self-assembly across multiple length scales. Herein, an exception is introduced, namely, aqueous dispersions of cellulose nanocrystals (CNCs) that form superstructured, adherent layers between solid surfaces upon confined evaporation-induced self-assembly (C-EISA). The inherently strong CNCs ( $E_A > 140$  GPa) align into rigid, nematically ordered lamellae across multiple length scales as a result of the stresses associated with confined evaporation. This long-range order produces remarkable anisotropic adhesive strength when comparing in-plane ( $\approx 7$  MPa) and out-of-plane ( $\leq 0.08$  MPa) directions. These adhesive attributes, resulting from self-assembly, substantially outperform previous biomimetic adhesives obtained by top-down microfabrication (dry adhesives, friction driven), and represent a unique fluid (aqueous)-based system with significant anisotropy of adhesion. By using C-EISA, new emergent properties will be closely tied with the nature of colloids and their hierarchical assemblies.

Self-assembly of natural and synthetic precursors may enable complex, multiscaled, phenomena with far-reaching implications.<sup>[1,2]</sup> Particularly, biological systems can assemble molecules into macroscopic materials, such as the pads of gecko feet composed of  $\beta$ -keratin hierarchically structured from spatulae to setae to adhesive lamellae.<sup>[3]</sup> In contrast, synthetic self-assembly still lacks the elegance to engineer such complex functional structures across multiple length scales. Still, fundamental advances in self-assembly revolutionize how we approach the study of colloids and interfaces, and regularly lead to numerous breakthroughs in cutting-edge applications.<sup>[2]</sup> Recently, the ordered and hierarchical assembly of colloids on surfaces or in suspension, has emerged as a promising route to engineer complex nano- and microstructures.<sup>[4-6]</sup> For example, suspensions of nanoparticles can assemble onto, and adhere to, soft materials (e.g., hydrogels and tissue) by exploiting multiple secondary interactions between nanoparticles and polymers.<sup>[7]</sup>

Dr. B. L. Tardy, L. G. Greca, Prof. O. J. Rojas  
Department of Bioproducts and Biosystems  
School of Chemical Engineering  
Aalto University  
02150 Espoo, Finland  
E-mail: blaise.tardy@aalto.fi; orlando.rojas@aalto.fi

Dr. J. J. Richardson, Prof. H. Ejima  
Department of Materials Engineering  
The University of Tokyo  
Tokyo 113-8656, Japan  
E-mail: ejima@material.t.u-tokyo.ac.jp

 The ORCID identification number(s) for the author(s) of this article can be found under <https://doi.org/10.1002/adma.201906886>.

© 2020 The Authors. Published by WILEY-VCH Verlag GmbH & Co. KGaA, Weinheim. This is an open access article under the terms of the Creative Commons Attribution-NonCommercial-NoDerivs License, which permits use and distribution in any medium, provided the original work is properly cited, the use is non-commercial and no modifications or adaptations are made.

Prof. J. Guo  
School of Biomass Science and Engineering  
Sichuan University  
Chengdu 610017, China

Prof. J. Guo  
Wyss Institute for Biologically Inspired Engineering  
John A. Paulson School of Engineering and Applied Sciences  
Harvard University  
Cambridge, MA 02138, USA

Prof. O. J. Rojas  
Department of Applied Physics  
School of Science  
Aalto University  
02150 Espoo, Finland

Prof. O. J. Rojas  
Departments of Chemical and Biological Engineering  
Chemistry and Wood Science  
University of British Columbia  
2360 East Mall, Vancouver, BC V6T 1Z4, Canada

DOI: 10.1002/adma.201906886

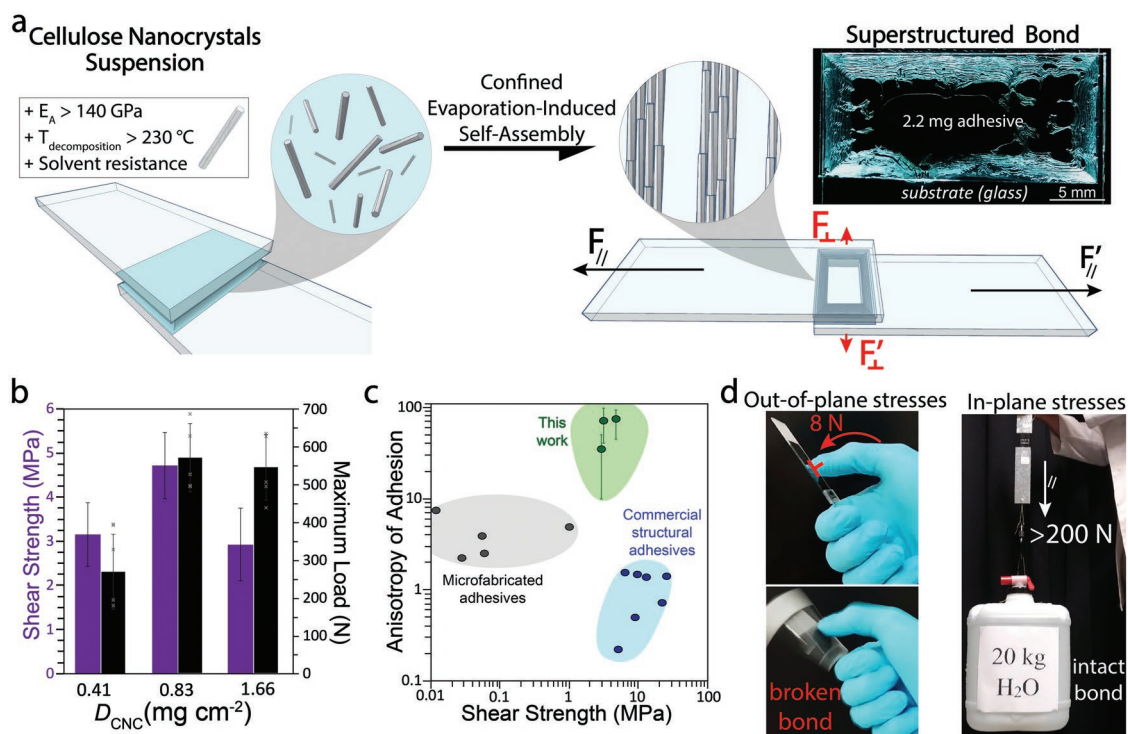


**Figure 1.** C-EISA between hydrophilic substrates (glass slides), resulting in adhesive, superstructured CNCs. a) Schematic illustration of the highly aligned, nematic, arrangement obtained by the self-assembly of CNCs during confined evaporation between hydrophilic substrates. The red and black arrows indicate anisotropic, out-of-plane, and in-plane forces, respectively. Right-hand side inset: example of superstructured bonds, with multiscaled and long-range order of CNCs, obtained from 2.2 mg of CNC suspended in 20  $\mu$ L of water and left to assemble between two glass plates. b) Adhesive shear strength for in-plane lap-shear and corresponding maximum loads for three values of  $D_{\text{CNC}}$ . Standard deviation (SD) is shown. c) Anisotropy as a function of shear strength for the adhesive conditions presented in this work (green, SD shown), microfabrication approaches (gray), and commercial glues such as those based on cyanoacrylate or epoxy. Corresponding references are detailed in Figure S7 in the Supporting Information. d) Illustration of the outstanding anisotropic adhesion achieved with 2.2 mg of CNCs with a contact area of  $\approx 1$  cm<sup>2</sup>: A one-handed, thumb press normal to the plane (out-of-plane) is sufficient to break the adhesive (Movie S3, Supporting Information). In contrast, a >200 N load in-plane (and up to 700 N according to lap shear tests) is supported.

The interfacial adhesion of hard nanoparticles with soft matter resulted in a new class of adhesive, contrasting substantially from conventional, covalent, approaches to adhesion.<sup>[8]</sup> Therefore, further progress in discovering new routes to achieve ordered structures, with appropriate building blocks, should lead to new functions, useful in various applications.

Emergent properties in self-ordered systems are tied to the physicochemical features of the building blocks (e.g., geometry, surface chemistry, strength), and a careful choice of the latter is crucial to achieve new functions in hierarchical assemblies. For instance, flexible yet strong rod-like polymeric nanoparticles will promote supramolecularly coherent adhesion between hard surfaces by maximizing interfacial contact.<sup>[9]</sup> However, there is still no route to assemble such building blocks into the appropriate hierarchical structures, across multiple length scales, to allow for strong adhesion. Such a colloid-centered framework is however reminiscent of what is observed in the animal kingdom (e.g., insects and reptiles), where highly anisometric, hierarchically structured setae maximize adhesion.<sup>[10,11]</sup> Analogous to biological systems, superstructured and nanoparticulated glues should allow for remarkable in-plane adhesive strength combined with weak out-of-plane adhesion.

Herein, we demonstrate that a single drop of a suspension of cellulose nanocrystals (CNCs; 134  $\pm$  52 nm in length<sup>[12]</sup>),

develops a highly ordered hierarchical structure that translates into strong anisotropic adherence between hard substrates upon confined evaporation-induced self-assembly (C-EISA). The confined evaporation of the CNC suspension (23 °C, 23% of relative humidity (RH)) results, simultaneously, in colloid–substrate and colloid–colloid supramolecular consolidation via cellulose–cellulose and cellulose–substrate interactions, combined with the formation of microscaled nematically ordered microstructures (Figure 1a). This leads to outstanding lap-shear adhesion, with an average strength of up to 4.7  $\pm$  0.7 MPa (reaching a maximum of 7 MPa, Figure 1b, and Discussion S1 and Movie S1, Supporting Information). These values are comparable to best-of-its-type commercial formulations such as Superglue.<sup>[13]</sup> Notably, the out-of-plane adhesion developed by CNC-based C-EISA is considerably lower, with adhesive strengths of 0.08 MPa (Movie S2, Supporting Information). Such adhesion anisotropy, extending far beyond adhesive properties expected from CNCs, is highly desirable in applications where reusability and protection of high value yet brittle elements are key.<sup>[14,15]</sup> Anisotropy in adhesive strength, calculated from the ratio between the in-plane and out-of-plane values, averaged 73  $\pm$  25, with a maximum of up to  $\approx 100$  (Figure 1c,d). The inherent properties of CNCs, such as high

strength (tensile strength up to 7 GPa, and  $E_A > 140$  GPa),<sup>[16,17]</sup> chemical resistance to most solvents, and high thermal stability ( $T_{\text{decomposition}} > 250$  °C),<sup>[18,19]</sup> highlight the exceptional resilience of such building-block, which usually represents a crucial requirement in the formation of structural components. Additionally, given that adhesive bonds are formed in the presence of the CNC counterion, sodium, the system is fully redispersible in water, and thus rebondable (Discussion S1, Supporting Information).<sup>[20]</sup> From its fundamental nature and broad practical implications, exploiting C-EISA to mimic biological structured adhesion offers an alternative to top-down lithography to generate anisotropic adhesives. The outstanding adhesive attributes also highlight the high potential for transferring colloid-scaled features to bring unique functionalities into macroscaled assemblies.

High hydrophilicity of the substrate is essential for developing the strong supramolecular interactions between colloid and substrate (Discussion S1c, Figure S1, and Table S1, Supporting Information). Anisotropic adhesion by C-EISA can also be applied to substrates of diverse geometry, porosity, and roughness. A 40% reduction in adhesion strength occurs when using micrometrically rough substrates (Figure S2 and Discussion S1a, Supporting Information), which result in lamellae with more squared cross-sections rather than the “meniscus-templated” cross-sections, as observed on smooth substrates.

The supramolecular self-cohesion of CNCs and their strong interaction with surfaces define the final adhesion strength (Discussion S1, Supporting Information). Hence, it is the contact area of the adhesive, within the overlap area, and the long-range order in the assembly that defines the strength rather than the initial concentration of the CNC suspension. The contact area of the adhesive and the long-range order are linked with the areal density of the deposited CNC in the overlap area ( $D_{\text{CNC}}$ ). For the overlap typically evaluated herein ( $1\text{--}1.5 \times 2.5$  cm<sup>2</sup>), a lower critical failure threshold at  $D_{\text{CNC}} \approx 20$  μg cm<sup>-2</sup>, below which robust adhesion does not occur as readily (Discussion S1a, Supporting Information), was observed. The contact area is  $\leq 1\%$  of the overlap area at such low  $D_{\text{CNC}}$ , this corresponds to a thickness of the adhesive layer  $\leq 1$  μm (Discussion S1, Supporting Information).

$D_{\text{CNC}}$  over the whole overlap area scaled logarithmically with the actual contact area between the CNCs and the substrate (Figure S3, Supporting Information; contact area (%) =  $15.54 \times \ln(D_{\text{CNC}}) + 48.6$ , with  $D_{\text{CNC}} > 0.05$  mg cm<sup>-2</sup>). Higher shear strength developed at higher  $D_{\text{CNC}}$  (Figure S3, Supporting Information), but after normalization to the contact area, the strength appeared to be of the same order, independent from the initial  $D_{\text{CNC}}$  (Discussion S1, Supporting Information). The highest shear strength was obtained at the two highest  $D_{\text{CNC}}$  when using gelled suspensions at the maximum CNC concentration tested, 11 wt%. Interestingly, although the hierarchically structured assembly would suggest multi-stage fracture propagation, only catastrophic bond rupture was observed (Figure S4a, Supporting Information). This is explained by the high strength and associated brittleness of the bond. Cohesive, in-plane shear failure of the bond was observed (Figure S5, Supporting Information). The high adhesion at the interface was evidenced by the rotation of the CNCs, when the shear force is orthogonal to the lamellae (Figure S5c, Supporting

Information). Under adhesive shear, the CNCs rotate toward the strain direction (Figure S5c,d, Supporting Information). This also emphasizes that the mechanism of adhesion is principally due to the friction generated by CNCs nematicallly arranged along the contour of the bond (Figure S6, Supporting Information), leading to unique property spaces for the CNC-based adhesive (Figure 1c and Discussion S1b and Figure S4b, Supporting Information). Interestingly, for samples equilibrated for 2 days at 82% RH, a marginal reduction of 8.6% in adhesive strength was observed (Discussion S1, Supporting Information). Collectively, the results suggest that adhesion arises when the high capillary stresses developing during C-EISA promote supramolecular bonds both between the particles themselves, and between the particles and substrates. These supramolecular bonds are the result of capillary forces overcoming the hydrogen-bonded layer of water to generate new H-bonds as well as Coulombic, and van der Waals interactions between particles, and with the substrates.<sup>[21,22]</sup>

The formation and long-range ordering of the superstructured adhesive occur during C-EISA, where CNCs accumulate toward, and orient parallel to the edges of the drying front. Such assembly is driven by the evaporative flux that follows the drying front, with a rate that is higher than required for equilibration of the colloidal suspension.<sup>[1]</sup> Contrary to previous reports that describe the formation of lamellae under confined EISA displaying a stick-and-slip behavior, i.e., by successive unpinning and repinning with intermediate material deposition,<sup>[23–25]</sup> the time-lapse observations of the CNCs superstructuring revealed a different mechanism (Movies S4–S7, Supporting Information). Here, the lamellae actually form by fracture generation and propagation in the gelled suspension followed by planar contraction of the fractured domains (Movies S4–S7, Supporting Information). No free CNCs are observed outside lamellae, suggesting a high internal cohesion of the receding lamellae (Figure 2a–c and Figure S5, Supporting Information). The lamellae also decrease in thickness closer to the center of the bonded area, likely due to the evaporation process proceeding from the edges inward (Figure S8, Supporting Information). The thickness and width of the micrometrically ordered lamellae (Figure 2d) decrease with  $D_{\text{CNC}}$ , with widths typically on the order of 50 μm and thicknesses ranging from  $\approx 10$  to 50 μm. The values correlate with the logarithmic relationship between the contact area and  $D_{\text{CNC}}$ , as described in Figure S3 in the Supporting Information.

C-EISA is proposed to develop through three distinct stages,  $t_1$ – $t_3$  (Figure 2e).  $t_1$ ) The drying front locally concentrates the CNCs and the suspension begins to recede toward the center of the contact area (Movies S4 and S5, Supporting Information).  $t_2$ ) As the CNC concentration reaches a critical threshold and the internal stresses in the principle plane overcome the cohesion of the gelled suspension, initiation and propagation of a fracture occurs, where two additional menisci appear in the propagating fracture (Movies S4 and S5, Supporting Information).  $t_3$ ) The CNCs lamella solidifies through supramolecular interactions that bring high internal cohesion and adhesion to the two surfaces via coupling of the capillary forces between CNCs and between CNCs and substrates (Movies S6 and S7, Supporting Information).<sup>[2,26,27]</sup> The supramolecular interactions associated with the polymeric nature of CNCs as well as their transversal

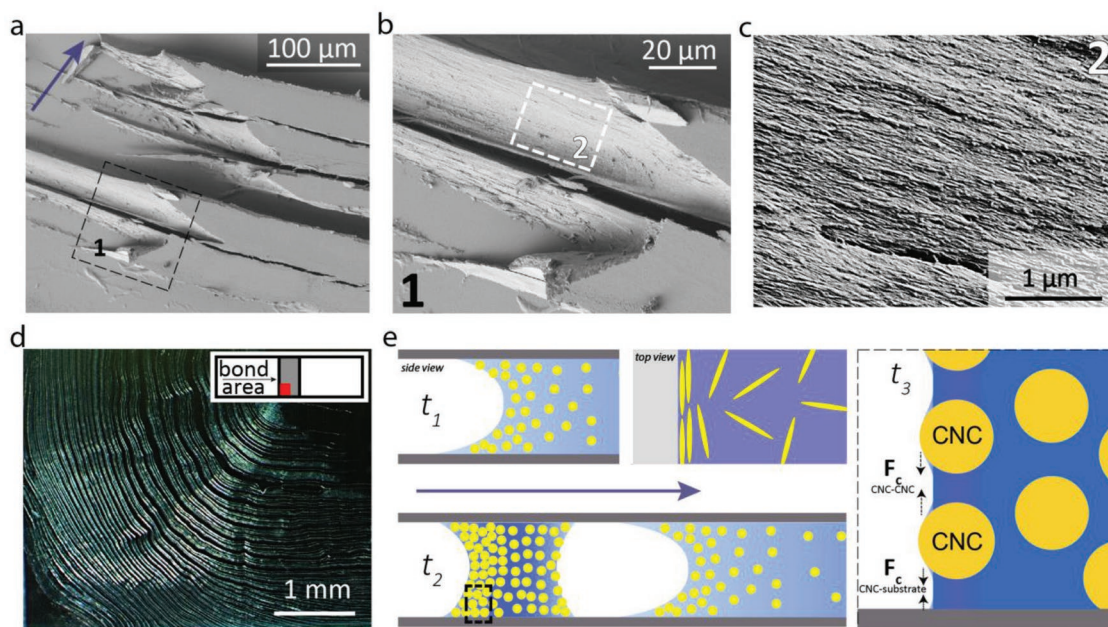


**Figure 2.** C-EISA resulting in superstructures across multiple length scales and schematics of the assembly mechanism. a) SEM images of lamellae presenting late (close-by lamellae) and early stage (spaced groups of lamellae) fractures between the lamellae. The arrow indicates the drying direction. b) Magnified view of area 1 in (a). c) Magnified view of area 2 in (b) highlighting highly aligned CNCs. d) A corner of the bonded area between two glass slides observed in dark field and shows the multiple, homogeneous lamellae formed. e) Schematic illustration of the assembly mechanism highlighting steps 1 to 3, as discussed in the main text.

flexibility depart significantly from other inorganic or hybrid colloids and enable them to maximize interfacial adhesion. In this process, the cellulose chains, which are initially highly aligned within the crystalline domains of each CNCs, end up aligned across the long axis of the lamellae. Therefore, because CNCs are aligned relative to each other within the lamellae, alignment from the molecular to the macroscale is achieved, similar to biological superstructuring in gecko feet (Figure 2 and Discussion S2, Supporting Information). This process also results in two types of lamellae cross-sectional profiles: symmetrical menisci and asymmetrical menisci (Figure S9a–d, Supporting Information, also visible in the edges of the lamellae in Figure 2a,b). As a result, the distance between lamellae follows a bimodal distribution, with large distances between lamellae resulting from early stage rupture and small distances between lamellae resulting from rupture of consolidated gels at later stages. Lamellae were also closer to each other toward the center of the rim. The cross-sectional morphology of the lamellae suggests an improved frictional effect due to the larger contact area from the preserved, highly wetting, meniscus shape. The alignment of cellulose chains at the surface of the aligned CNCs maximizes the directionality of the frictional response of the strained adhesive.<sup>[28]</sup> Alignment is also visible on the top of the lamellae when observed after out-of-plane fracture (Figure S9e,f, Supporting Information). Such effects have been previously demonstrated for the top-down fabrication of superstructured adhesives, but until now eluded bottom-up fabrication.<sup>[29,30]</sup> Furthermore, the bottom-up self-assembly of polymeric colloids offers a more amenable and accessible process to generate and study anisotropic adhesion. For instance, the strategy presented herein also outperforms anisotropic adhesives obtained from

chemical vapor deposition (shear strength up to 1 MPa and anisotropy of adhesion below 6).<sup>[31]</sup>

The process is entirely green as it uses bio-colloids and water for the formation of the adhesive layer. However, the assembly duration is relatively high (bonding time between 2 and 6 h) compared with some structural adhesives or micro-fabricated dry adhesives (bonding time of a few seconds), but relatively shorter than more common structural adhesives that cure over 24 h. However, the evaporative flux density distribution across the evaporating interface under confinement having a higher degree of symmetry compared, for instance, with sessile drops<sup>[32]</sup> suggests that increasing evaporation rate with temperature or by adding co-solvents would still result in highly ordered microstructures. This is further supported by the apparent absence of chiral nematic order even in samples assembled from fully dispersed solutions, suggesting a dominant effect from the drying fluxes. Increasing the evaporation rate by forming the adhesive layer at 50 °C and RH < 23% resulted in smaller contact areas, with less defined lamellae, and a slightly reduced adhesion strength. Well-defined lamellae and a larger contact area were obtained for adhesive layers formed at 23 °C and 50% RH (Figure S10, Supporting Information). For  $D_{\text{CNC}} = 0.33 \text{ mg cm}^{-2}$ , contact areas of  $34.0 \pm 4.4\%$  and  $30.0 \pm 4.4\%$  were observed for the bonds formed at 23 °C and 50% RH or 50 °C and RH < 23%, respectively. Accordingly, the maximum loads in-plane were  $406 \pm 153$  and  $361 \pm 53$  N. These differences highlight the importance of the interplay between wetting and long-range order.<sup>[33]</sup>

The transition to step  $t_2$  is critical for the superstructuring and the final strength of the adhesive, and is most crucially associated with the drying-induced alignment of CNCs as evidenced

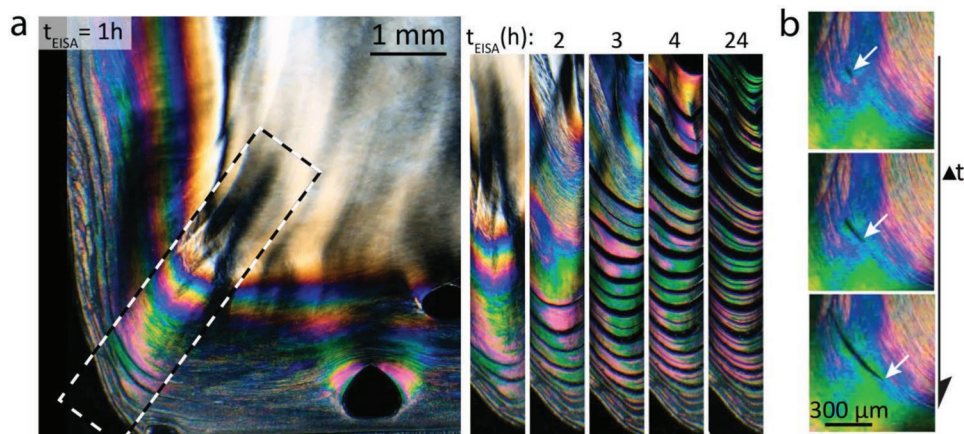


**Figure 3.** Mechanistic insights on the formation of CNC superstructures as demonstrated by polarized microscopy (bond of 2.5 cm<sup>2</sup> and 5.5 mg of CNCs). a) Images obtained between cross-polarizers after 1 h of C-EISA in a corner of the bonding area (left) and corresponding time-lapse of retardation colors developing during C-EISA and bond formation (right). Lamellae formation and planar contraction can be clearly observed. The voids present at the bottom right correspond to adventitious bubbles present during bond formation. b) Fracture initiation and propagation during steps  $t_{2-3}$ . The white arrow indicates propagation, and the associated increase in retardation color.

by imaging between cross-polarizers (**Figure 3a** and Discussion S2 and Movies S4–S7, Supporting Information).<sup>[34,35]</sup> The CNC gel (11%) was originally quasi-isotropic (i.e., appearing black), but as the suspension dried, a high alignment of the nanocrystals was observed, initially increasing from the center to the edge of the bonding. The order of the colors observed after complete drying points to an increase in retardation of up to fourth and close to the fifth order, as extrapolated from a Michel–Lévy chart.<sup>[36]</sup> Given an average birefringence of 0.55 for CNCs and a thickness of the lamellae between 10 and 40  $\mu\text{m}$  (from the inner to the outer lamellae, Figures S5, S8, S9, and S11 in the Supporting Information, which includes a Michel–Lévy chart for reference), the fourth-order retardation colors indicate a near complete alignment of the CNCs within each lamellae. This highlights the outstanding effect of confinement on the alignment of the nanocrystals.<sup>[34,36,37]</sup> Upon reaching second- to third-order interference colors, fracture initiation and propagation occurs and large lamellae are formed that will contract significantly during step  $t_3$  of the C-EISA process (**Figure 3a**). During the later stages of C-EISA, fracturing events lead to a substantial increase of order due to the high internal stress of the concentrating lamellae, as the viscoelastic stresses are released and enable further in-plane compression of the lamellae and alignment of the CNCs within each lamella (**Figure 3b** and **Figure S12**, Supporting Information). The low initial internal stresses cause a slower early fracture propagation (several hours). In contrast, it takes only several minutes for the late-stage fractures, due to the low energy cost of fracture propagation alongside highly nematically ordered lamellae that consist of concentrated gels.

Once the strong water–cellulose interaction is overcome by capillary forces,<sup>[22,38]</sup> high-strength supramolecular bonds are formed, bringing extremely high cohesion to the nematically aligned CNC lamellae, as seen by in situ small-angle X-ray scattering (SAXS) and in situ THz/far-IR spectroscopy (Far-IR) (**Figure 4a–c**). The three steps of assembly were apparent from both techniques, but different important phenomena could be seen by using each of these techniques. Specifically, Far-IR

indicated bond-angle deformation and internal rotation/torsion modes relating to hydrogen bonding as they generally appear below 400 cm<sup>-1</sup>. SAXS elucidated the orientation and packing of the CNCs at longer camera lengths. For example, SAXS demonstrated that in step  $t_1$ , the CNC interparticle distances rapidly decrease near the air–water interface (**Figure 4a** and **Figure S13**, Supporting Information). Step  $t_2$  is visible by the increased orientation and packing, along with the appearance of microvoids (fractures), while step  $t_3$  appears as a decrease in overall scattering due to the drying (**Figure 4a** and **Figure S14**, Supporting Information). SAXS also highlights that step  $t_3$  could be observed as spatially separated points moving from the interior of the drying overlap region (undergoing step 1) toward the outside edge of the bonded area (completing step  $t_3$ ) (**Figure 4b** and **Figure S15**, Supporting Information). Far-IR demonstrated a period of hydration (step  $t_1$ ) without significant changes in molecular attraction, followed by a rapid transition stage (step  $t_2$ ) where the CNC lamellae start to form, as seen through a reduction in molecular torsion and the generation of inter- and intramolecular bonds (**Figure 4c** and **Figure S16** and **Table S2**, Supporting Information). Finally, the absorption peaks shift, likely due to increased packing and the resultant strain/stress on the CNCs from the long-ranged order and interparticle attraction as the suspension dries (step  $t_3$ ; **Figure S16**, Supporting Information). Cross-correlated SAXS/Far-IR, as obtained by 2D synchronous analysis, demonstrates that molecular and physical changes occur simultaneously during C-EISA. The orientation of the CNCs follows the lamella direction as seen in SEM and corresponds with Hermans orientation function values  $> 0.9$  as derived from SAXS (**Figure 4a–c** and **Figure S17**, Supporting Information). The concentration did not strongly affect the alignment, which agreed with the fact that the CNCs have a low critical  $D_{\text{CNC}}$ , as there are no intermediate adhesion states. This was also seen in the stress–strain curves when the substrates were pulled in-plane, as it proceeded in a linear fashion followed by critical failure of the adhesive with the complete separation of the adhered substrates in a single, rapid step (**Figure S4a**, Supporting Information).

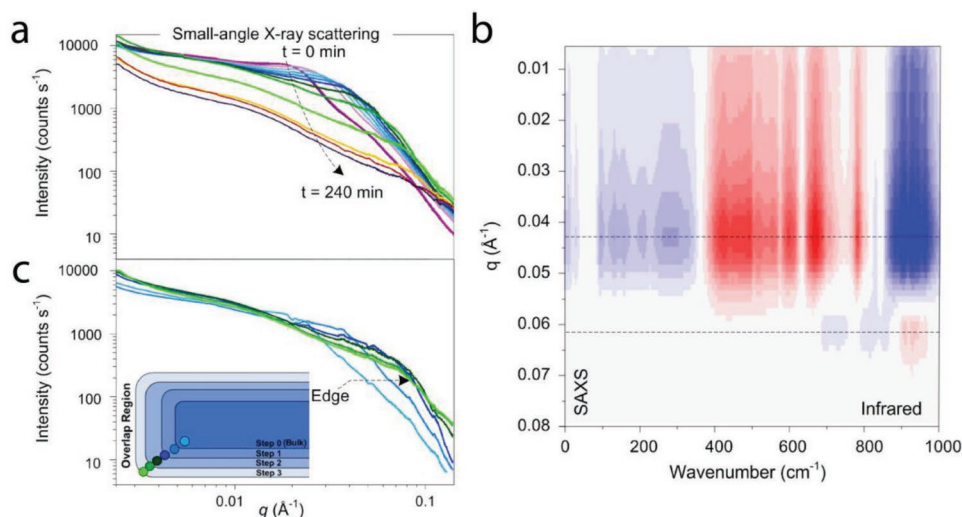


**Figure 4.** Mechanistic insights on the formation of CNC superstructures as demonstrated by SAXS and Far-IR (bond of 2.5 cm<sup>2</sup> and 3.3 mg of CNCs). a) Scattering evolution over time of the CNCs during C-EISA between two glass slides. The color coding indicates the time progression following the visible spectrum (rainbow), i.e., indigo ( $t = 0$  min) to deep red/maroon ( $t = 240$  min). b) Position-dependent order during C-EISA between two glass slides ( $t = 1$  h). Moving from gel inward to the structured adhesive in steps  $t_2$  to  $t_3$ : Light blue (bulk), blue, dark blue, dark green, green, light green (step  $t_3$ ). c) Cross-correlation between physical superstructuring and evolution of molecular interactions as measured by in situ Far-IR and SAXS during C-EISA. The red and blue indicate cross-correlated and anti-correlated changes, respectively. The full Far-IR data are described in Figure S16 in the Supporting Information.

In conclusion, we demonstrate that a simple self-assembly phenomenon involving aqueous suspensions of anisotropic organic nanoparticles can induce extremely high, noncovalent adhesive shear strength. C-EISA resulted in a gel-to-solid transition forming multiscaled order, with superstructured lamellae that act in a fashion similar to most dry and reversible bioadhesives found in nature, for instance in setae of insects or geckos. Analogous to natural reversible adhesives, the in-plane and out-of-plane adhesion values diverge by more than 70-fold. Importantly, the internal structure of the adhesive is tightly bound to the C-EISA phenomenon, which opens routes for further exploring both the adhesive properties using, for instance, specific bond contour, the superstructuring of other anisotropic polymeric colloids, or control over superstructure formation.<sup>[25]</sup> Additionally, the vast realm of self-assembly associated with mesoscaled capillary forces<sup>[39,40]</sup> means that C-EISA, will find use, e.g., in introducing higher order in hierarchical assemblies or in promoting other emergent properties, such as piezoelectricity.<sup>[41]</sup> The time required for the formation of the adhesive layer by C-EISA poses a restriction compared with some commercial structural adhesives and dry adhesives that form bonds within seconds. However, the prospects of using fully green, cost-effective, and aqueous-based systems are very appealing. The effect of faster evaporation rates can be considered in future developments. On the other hand, the rebondable nature of the adhesives, also previously demonstrated for synthetic systems obtained by top-down fabrication,<sup>[42]</sup> may be further tethered by judicious use of counterions, which could also provide control over the humidity response of the adhesives.<sup>[43,44]</sup> The reversible assembly of the adhesive also offers a potential for decreased permanent damage to the assembled elements and for increased sustainability.<sup>[14,15]</sup> Lastly, with the ongoing mass production of CNCs,<sup>[45]</sup> and the implementation of a vast range of chemical modifications of nanocelluloses,<sup>[46]</sup> the high strength and high anisotropy of adhesion

demonstrated herein will significantly impact the development of high-performance, green, structural adhesives in a wider range of applications and substrates. New potential applications can be envisioned to be associated with the outstanding anisotropy of adhesion. For instance, CNC-based adhesives applied onto high-strength, yet brittle, high-value machine parts or construction elements is expected to prevent failure and improve reusability. Overall, this study unveils a unique aspect of superstructured adhesives from naturally obtained polymeric colloids assembled under C-EISA and, as a new paradigm, it highlights various avenues for potential applications and further processing.

## Supporting Information

Supporting Information is available from the Wiley Online Library or from the author.

## Acknowledgements

B.L.T. and J.J.R. contributed equally to this work. The authors acknowledge the funding support by the European Research Commission for the H2020-ERC-2017-Advanced Grant “BioELCell” (788489). L.G.G. acknowledges funding by the Aalto University School of Chemical Engineering doctoral programme. The authors are thankful for discussions with Prof. Ikkala, within their Academy of Finland Centre of Excellence on “Molecular Engineering of Biosynthetic Composite Materials Research” (HYBER). Part of this research was undertaken on the small-/wide-angle X-ray scattering beamline at the Australian Synchrotron, part of ANSTO.

## Conflict of Interest

The authors declare no conflict of interest.

## Keywords

adhesion, cellulose, colloids, self-assembly, supramolecular interactions

Received: October 20, 2019

Revised: December 16, 2019

Published online: February 16, 2020

- 
- [1] R. D. Deegan, O. Bakajin, T. F. Dupont, G. Huber, S. R. Nagel, T. A. Witten, *Nature* **1997**, 389, 827.
- [2] N. Mittal, F. Ansari, V. Gowda Krishne, C. Brouzet, P. Chen, P. T. Larsson, S. V. Roth, F. Lundell, L. Wågberg, N. A. Kotov, L. D. Söderberg, *ACS Nano* **2018**, 12, 6378.
- [3] Y. Min, M. Akbulut, K. Kristiansen, Y. Golan, J. Israelachvili, in *Nanoscience and Technology: A Collection of Reviews from Nature Journals* (Ed: P. Rodgers), World Scientific, Singapore **2009**, p. 38.
- [4] J. Guo, B. L. Tardy, A. J. Christofferson, Y. Dai, J. J. Richardson, W. Zhu, M. Hu, Y. Ju, J. Cui, R. R. Dagastine, I. Yarovsky, F. Caruso, *Nat. Nanotechnol.* **2016**, 11, 1105.
- [5] A. A. Shah, B. Schultz, W. Zhang, S. C. Glotzer, M. J. Solomon, *Nat. Mater.* **2015**, 14, 117.
- [6] S. C. Glotzer, M. J. Solomon, *Nat. Mater.* **2007**, 6, 557.
- [7] S. Rose, A. PrevotEAU, P. Elzière, D. Hourdet, A. Marcellan, L. Leibler, *Nature* **2014**, 505, 382.
- [8] K. Kendall, *Science* **1994**, 263, 1720.
- [9] S. Sacanna, M. Korpics, K. Rodriguez, L. Colón-Meléndez, S. H. Kim, D. J. Pine, G. R. Yi, *Nat. Commun.* **2013**, 4, 1688.
- [10] H. Gao, X. Wang, H. Yao, S. Gorb, E. Arzt, *Mech. Mater.* **2005**, 37, 275.
- [11] E. Arzt, S. Gorb, R. Spolenak, *Proc. Natl. Acad. Sci. USA* **2003**, 100, 10603.
- [12] K. W. Klockars, B. L. Tardy, M. Borghei, A. Tripathi, L. G. Greca, O. J. Rojas, *Biomacromolecules* **2018**, 19, 2931.
- [13] P. Klemarczyk, J. Guthrie, in *Advances in Structural Adhesive Bonding* (Ed: D. Dillard), Woodhead Publishing Limited, Cambridge, UK **2010**, p. 96.
- [14] A. Sev, *Sustainable Dev.* **2009**, 17, 161.
- [15] W. R. Stahel, *Nature* **2016**, 531, 435.
- [16] A. Šturcová, G. R. Davies, S. J. Eichhorn, *Biomacromolecules* **2005**, 6, 1055.
- [17] R. J. Moon, A. Martini, J. Nairn, J. Simonsen, J. Youngblood, *Chem. Soc. Rev.* **2011**, 40, 3941.
- [18] M. V. Ramiah, *J. Appl. Polym. Sci.* **1970**, 14, 1323.
- [19] T. Liebert, in *Cellulose Solvents: For Analysis, Shaping and Chemical Modification* (Eds: T. Liebert, T. Heinze, K. Edgar), ACS, Washington, DC, USA **2010**, p. 3.
- [20] S. Beck, J. Bouchard, R. Berry, *Biomacromolecules* **2012**, 13, 1486.
- [21] S. M. Notley, B. Pettersson, L. Wågberg, *J. Am. Chem. Soc.* **2004**, 126, 13930.
- [22] R. Parthasarathi, G. Bellesia, S. P. S. Chundawat, B. E. Dale, P. Langan, S. Gnanakaran, *J. Phys. Chem. A* **2011**, 115, 14191.
- [23] W. Han, Z. Lin, *Angew. Chem., Int. Ed.* **2012**, 51, 1534.
- [24] Y. Lin, Z. Su, G. Xiao, E. Balizan, G. Kaur, Z. Niu, Q. Wang, *Langmuir* **2011**, 27, 1398.
- [25] R. D. Deegan, *Phys. Rev. E: Stat. Phys., Plasmas, Fluids, Relat. Interdiscip. Top.* **2000**, 61, 475.
- [26] B. L. Tardy, B. D. Mattos, L. G. Greca, T. Kämäräinen, K. W. Klockars, O. J. Rojas, *Adv. Funct. Mater.* **2019**, 29, 1808518.
- [27] Y. Zhao, W. Li, X. Jiang, F. Li, X. Li, W. Zhang, J. Sen Jiang, J. Liu, K. Ariga, M. Hu, *ACS Nano* **2017**, 11, 3662.
- [28] Y. Mo, K. T. Turner, I. Szlufarska, *Nature* **2009**, 457, 1116.
- [29] D. Brodoceanu, C. T. Bauer, E. Kroner, E. Arzt, T. Kraus, *Bioinspiration Biomimetics* **2016**, 11, 051001.
- [30] L. Heepe, S. N. Gorb, *Annu. Rev. Mater. Res.* **2014**, 44, 173.
- [31] L. Qu, L. Dai, M. Stone, Z. Xia, L. W. Zhong, *Science* **2008**, 322, 238.
- [32] K. W. Klockars, N. E. Yau, B. L. Tardy, J. Majoinen, T. Kämäräinen, K. Miettunen, E. Boutonnet, M. Borghei, J. Beidler, O. J. Rojas, *Cellulose* **2019**, 26, 491.
- [33] I. Hoeger, O. J. Rojas, K. Efimenko, O. D. Velev, S. S. Kelley, *Soft Matter* **2011**, 7, 1957.
- [34] J. Kennedy, *Carbohydr. Polym.* **2000**, 43, 206.
- [35] B. L. Tardy, M. Ago, J. Guo, M. Borghei, T. Kämäräinen, O. J. Rojas, *Small* **2017**, 13, 1702084.
- [36] B. E. Sørensen, *Eur. J. Mineral.* **2013**, 25, 5.
- [37] E. D. Cranston, D. G. Gray, *Colloids Surf., A* **2008**, 325, 44.
- [38] R. Sinko, X. Qin, S. Ketten, *MRS Bull.* **2015**, 40, 340.
- [39] M. Mastrangeli, *Adv. Mater.* **2015**, 27, 4254.
- [40] V. Flauraud, M. Mastrangeli, G. D. Bernasconi, J. Butet, D. T. L. Alexander, E. Shahrabi, O. J. F. Martin, J. Brugger, *Nat. Nanotechnol.* **2017**, 12, 73.
- [41] L. Csoka, I. C. Hoeger, O. J. Rojas, I. Peszlen, J. J. Pawlak, P. N. Peralta, *ACS Macro Lett.* **2012**, 1, 867.
- [42] H. Cho, G. Wu, J. C. Jolly, N. Fortoul, Z. He, Y. Gao, A. Jagota, S. Yang, *Proc. Natl. Acad. Sci. USA* **2019**, 116, 13774.
- [43] M. Shimizu, T. Saito, A. Isogai, *J. Membr. Sci.* **2016**, 500, 1.
- [44] T. Benselfelt, M. Nordenström, S. B. Lindström, L. Wågberg, *Adv. Mater. Interfaces* **2019**, 6, 1900333.
- [45] M. S. Reid, M. Villalobos, E. D. Cranston, *Langmuir* **2017**, 33, 1583.
- [46] Y. Habibi, *Chem. Soc. Rev.* **2014**, 43, 1519.

Minerva Access is the Institutional Repository of The University of Melbourne

**Author/s:**

Tardy, BL; Richardson, JJ; Greca, LG; Guo, J; Ejima, H; Rojas, OJ

**Title:**

Exploiting Supramolecular Interactions from Polymeric Colloids for Strong Anisotropic Adhesion between Solid Surfaces

**Date:**

2020-04-09

**Citation:**

Tardy, B. L., Richardson, J. J., Greca, L. G., Guo, J., Ejima, H. & Rojas, O. J. (2020). Exploiting Supramolecular Interactions from Polymeric Colloids for Strong Anisotropic Adhesion between Solid Surfaces. *Advanced Materials*, 32 (14), <https://doi.org/10.1002/adma.201906886>.

**Persistent Link:**

<http://hdl.handle.net/11343/252340>

**File Description:**

Published version

**License:**

cc-by-nc-nd